In vivo study of self-assembled alkylsilane coated degradable magnesium devices

Avinash Patil,[1,2] Samer H. Zaky,[2,3,4] Rong Chong,[2,3] Kostas Verdelis,[2,3,5] Elia Beniash[1,2,3,4]

[1]Department of Bioengineering, University of Pittsburgh, Pittsburgh, Pennsylvania 15261
[2]Center for Craniofacial Regeneration, University of Pittsburgh, Pittsburgh, Pennsylvania 15261
[3]Department of Oral Biology, School of Dental Medicine, University of Pittsburgh, Pittsburgh, Pennsylvania 15261
[4]Department of Restorative Dentistry, University of Pittsburgh, Pittsburgh, Pennsylvania 15261
[5]McGowan Institute for Regenerative Medicine, University of Pittsburgh, Pittsburgh, Pennsylvania 15219

Abstract: Magnesium (Mg) and its alloys are candidate materials for resorbable implantable devices, such as orthopedic devices or cardiovascular stents. Mg has a number advantages, including mechanical properties, light weight, its osteogenic effects and the fact that its degradation products are nontoxic and naturally present in the body. However, production of H_2 gas during the corrosion reaction can cause formation of gas pockets at the implantation site, posing a barrier to clinical applications of Mg. It is therefore desirable to develop methods to control corrosion rate and gas pocket formation around the implants. Here we evaluate the potential of self-assembled multilayer alkylsilane (AS) coatings to control Mg device corrosion and formation of gas pockets in vivo and to assess effects of the AS coatings on the surrounding tissues in a subcutaneous mouse model over a 6 weeks' period. The coating significantly slowed down corrosion and gas pocket formation as evidenced by smaller gas pockets around the AS coated implants (ANOVA; $p = 0.013$) and decrease in the weight loss values (t test; $p = 0.07$). Importantly, the microCT and profilometry analyses demonstrated that the coating inhibited the pitting corrosion. Specifically, the roughness of the coated samples was ~30% lower than uncoated specimen ($p = 0.02$). Histological assessment of the tissues under the implant revealed no inflammation or foreign body reaction. Overall, our results demonstrate the feasibility of use of the seld assembled AS coatings for reduction of gas pocket formation around the resorbable Mg devices. © 2018 Wiley Periodicals, Inc. J Biomed Mater Res Part B: Appl Biomater 107B: 342–351, 2019.

Key Words: magnesium, corrosion, coating, roughness, degradable implant, alkylsilane, self-assembly, toxicity

---

INTRODUCTION

Magnesium (Mg) and its alloys has emerged as promising materials for resorbable orthopedic devices due to their degradability in the body which eliminates the need for an implant removal surgery.[1–5] Mg is light-weight and its mechanical properties closely match those of bone. Divalent Mg^{2+} ion is one of the essential ions and its corrosion products—MgO and $Mg(OH)_2$ are safe and can be cleared from the body. Mg is highly biocompatible and several studies showed that Mg^{2+} ions can induce new bone formation.[6,7] However, one of the obstacles for use of Mg in clinical application is its initial rapid corrosion reaction leading to the formation of hydrogen (H_2) which creates gas pockets around the implanted Mg devices. Pure Mg readily corrodes when in contact with an aqueous solution and as shown in Eq. (1) H_2 gas is one of the reaction products:

$$Mg\,(s) + 2H_2O\,(aq) = Mg^{2+}(aq) + 2OH^-(aq) + H_2(g) \quad (1)$$
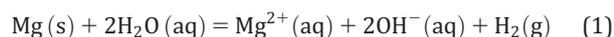
In addition to H_2, a complex mixture of insoluble Mg corrosion products forms in biological electrolytes in vivo and in vitro which consist of mineral salts, oxides and hydroxides which form a passivating layer around the corroding metal,[8,9] leading to the decrease of the corrosion rate. This passivating layer act as a barrier for diffusion of water toward the corroding metal leading to the decrease of its corrosion rate.[10,11] A portion of H_2 gas is absorbed in the surrounding tissues and blood, while the remaining H_2 forms pockets surrounding the implant.[12] Although, H_2 escapes the body quickly it is exchanged with other gases in vivo.[12] Attempts to use Mg as a material for resorbable devices can be traced to the 19th century, however the problem of gas pocket formation and other issues created obstacles for a widespread use of these devices in clinical practice.[13–15] Patient discomfort and gas embolism are two main clinical consequences of H_2 accumulation in body.[9] The gas pocket formed in tissue can slow down the tissue healing

process and the rapid degradation of implants may initiate an inflammatory response in surrounding tissues.[16,17] It is therefore important to control the Mg device degradation rate to improve clinical outcomes.[17] Ideally, the degradation rate should be such that H_2 produced is absorbed by surrounding tissues and rapidly accumulating degradation products will not cause inflammatory response.[9,12,18] With time the corrosion products forming around the device lower its degradation rate, however, it is highly desirable to prevent the initial corrosion burst.[12,19] More rapid degradation of Mg implant can occur during the initial period of implantation because of accumulation of body fluids around the implant due to trauma or surgery so it is important to control the H_2 gas evolution in the early period of implantation. To overcome the issue of the initial rapid corrosion and the H_2 burst leading to the formation of the gas pockets, three different strategies were used, namely, alloying, surface treatment and surface coating.[20,21] A variety of surface coating materials is used to control degradation of Mg including polymers,[22,23] calcium phosphate,[24] and polysiloxanes.[25–27]

Polysiloxanes have a number of advantages over other coating technologies, such as their well established chemistry,[28] biocompatibility,[29] and the potential for the surface functionalization of the coatings.[30] A good coating system should have optimum thickness, strong adhesion to substrate and defect free.[31] The polysiloxane coating satisfy all the above requirements. Polysiloxanes were used as anticorrosion coatings for metals, such as steel, aluminum, and iron and more recently they were used to control corrosion of resorbable Mg devices.[32–34]

Alkylsilane (AS), hybrid organosiloxanes, comprising hydrolysable siloxane head and hydrophobic alkyl tail, which upon hydrolysis become amphiphilic.[35] The amphiphilic properties of alkylsilane monomers can be harnessed to create self-assembled nanomaterials, including lamellar and other ordered structures.[30,36] Importantly, upon self-assembly the siloxane groups polymerize creating mechanicaly stable structures. We recently developed a micron thick self-assembled multilayer AS coatings for resorbable Mg devices,[37] which have a number of important advantages. Despite the fact that these coatings are only micron thick they are superior to polymer and calcium phosphate coatings in controlling Mg corrosion and reduction of H_2 production.[37] In addition, the hydroxyl groups of hydrolyzed AS molecules form covalent bonds with hydroxyl groups on metal surfaces providing much stronger adhesion to the substrate in comparison to other coatings.[32,38–40] In addition, Importantly, the *in vitro* tissue culture experiments also demonstrated a good cytocompatibility of these coatings.[37]

The aim of the present study was to test the hypothesis that the self-assembled AS coatings can control gas pocket formation and corrosion of the implanted Mg in a mouse subcutaneous model over a 6 weeks period.

MATERIALS AND METHODS

All the reagents were purchased from Sigma Aldrich (St. Louis, MO) and used as received unless otherwise stated. The Mg disc preparation, synthesis and deposition of the self-assembled multilayer AS coatings was conducted as described previously and is briefly outlined below.[37]

Metal disc preparation

Six mm diameter discs were stamped from 1 mm thick Mg (99.9% purity) sheet (Alfa Aesar, Ward Hill, MA) and polished with 1200 grit (5 μm) MicroCut® SiC abrasive discs (Buehler, Lake Bluff, IL), followed by etching in a solution comprising 20 mL 85% glycerol, 5 mL 65% HNO_3, and 5 mL glacial acetic acid for 60 s. The discs were sonicated in acetone for 30 min and stored under vacuum until further use. Prior to the AS coating, a thin uniform hydroxide layer was formed on the discs by immersion in 3.0M sodium hydroxide (NaOH) solution for 2 h. In addition to the passivating properties, $MgOH_2$ provides the substrate for covalent binding of the silanes to a surface.[25,41,42]

Synthesis and deposition of self-assembled multilayer AS coatings on Mg discs

Self-assembled multilayer alkylsilane (AS) films on Mg was prepared by a dip-coating technique as described elsewhere.[36,43,44] The precursor solution was prepared by mixing 0.25 mL (0.73 mM) n-decyltriethoxysilane (DTEOS) (Alfa Aesar, Ward Hill, MA), 0.43 mL (2.92 mM) tetramethoxysilane (TMOS) (Alfa Aesar, Ward Hill, MA), 2 mL (0.032 mM) of ethanol and 0.25 mL 0.010 mM HCl (aq.). The precursor solution was stirred for 24 h at room temperature to induce hydrolysis of DTEOS and TMOS. Mg discs passivated with NaOH were dip coated in the solution for 1 min and dried in air for 10 min at room temperature. The discs were subsequently dried in an incubator at 37°C for 24 h for removal of any trace amount of organic solvents.

Two groups of samples were used in this study as follows:

- Polished, etched and NaOH treated Mg disc (Mg-OH)
- AS coated NaOH treated Mg disc (Mg-OH-AS)

Surgical procedure

The University of Pittsburgh's Institutional Animal Care and Use Committee approved all animal studies. Eight-weeks old, five male SKH1-Elite hairless mice of albino background (stain Code- 477) from Charles River Laboratories International (Wilmington, MA, USA) were used for this study. Prior to surgery the mice were placed on a prewarmed heating pad to reduce hypothermia and decrease metabolic rate. Surgery took place under isofluorane inhalation anesthesia. The skin of the mouse was cleaned with alcohol swab and a 6 mm incision was made on its back. The noncoated and AS coated Mg discs were weighed prior to implantation and implanted subcutaneously on the left and right dorsal side of the mouse in the midsection of the body. The discs were inserted through the incision in the mid-sagittal plane of the animals and placed ~5 mm away from the spine. The incision was closed using coated VICRYL™ plus antibacterial (polyglactin 910) suture (Ethicon, Johnson & Johnson, New Brunswick, NJ). After surgery, the animals were given water

containing Silapap liquid containing 160 mg/mL Acetaminophen (National Drug Code-54838-0144-40; Silarx Pharmaceuticals, Carmel, NY) as an analgesic for 2 days and then all mice were placed on normal diet and water until the end of study. All animals were observed every day and received day-to-day managed care through the Division of Laboratory Animal Resources (DLAR) facility of the University of Pittsburgh. The *in vivo* experiment was carried out for 6 weeks after which mice were euthanized.

Assessment of the gas pocket formation

The formation of a gas pockets around the implanted discs was monitored by visual observation and images were taken every week with a digital camera every week throughout the experiment. The diameter of the gas pockets was measured from the images using ImageJ image processing package (ImageJ, Bethesda, MD).

Postmortem whole animal μCT analysis

Immediately after euthanasia, the μCT scans of the implantation sites containing the discs were performed using Viva-CT40 μCT scanner (Scanco Medical, Brutisselen, Switzerland) with 30 μm voxel size and a 70 kvp beam energy (200 ms exposure, 1 frame per view).

Optical microscopy analysis of the samples

The discs surface microstructures were observed using the Greenough stereo microscope Leica S8 APO equipped with Leica DFC295 digital microscope color camera (Leica Microsystems, Buffalo Grove, IL) prior to implantation, immediately after retrieving the discs from the subcutaneous site at 6 weeks postimplantation and after removal of the corrosion products (see "**The weight loss analysis of corroded discs**"). The light intensity and exposure settings were maintained the same for all images.

Histological analysis

After the Mg discs were retrieved, soft tissues beneath the Mg discs were carefully collected and immersed in 10% ethylenediaminetetraacetic acid (EDTA) (in $0.1M$ phosphate buffer, pH 7–8 for approximately 72 h, solution changed every 24 h and fixed in 10% neutral buffered formalin for 24 h prior to embedding. Fixed samples were placed in Tissue-Tek® MESH Biopsy Cassette (Sakura Finetek, Torrance, CA) and processed in a fully automated Leica ASP300 S tissue processor (Leica Biosystems, Buffalo Grove, IL). After paraffin infiltration, samples were placed in a mold and embedded in paraffin using Leica EG1160 paraffin embedding station (Leica Biosystems, Buffalo Grove, IL). The embedded specimens were cut into 5 μm thick sections using a Leica RM2255 fully automated rotary Microtome (Leica Biosystems Inc., IL) and mounted on a glass slide. The sections were H&E stained and observed using Nikon TE2000 microscope (Nikon Instruments, Melville, NY) in a bright field mode. The images were captured and analyzed using Nikon NIS Elements software.

The weight loss analysis of corroded discs

Prior to the experiments each disc was weighed using microbalance Mettler Toledo XPE26 (Mettler Toledo, Columbus, OH). After retrieving the discs from subcutaneous pouch the soft tissues attached to discs were removed carefully and the discs were cleaned in a 180 g/L CrO_3 solution to remove the corroded products. The discs were weighed and the % weight loss was calculated for each disc

High-resolution micro-computerized tomography (μCT) analysis of the samples

To assess the corrosion damage to the implant surface high resolution μCT was carried out. The discs were scanned before and after surgery. The extracted discs were cleaned with CrO_3 as described in section "**The weight loss analysis of corroded discs**". Prior to scanning the discs were packed in a plastic tube and separated by Parafilm spacers to avoid overlap. The discs were scanned on a Skyscan 1172 (Bruker-Skyscan, Contich, Belgium) μCT system prior to implantation and postretrieval after 6 weeks *in vivo*. The scans were conducted with an eight-micron voxel size (180 degree-angular range) and a 60 KVp beam energy with the use of a 0.5 mm Al filter, 400 ms exposure time, and 12 frames per view. The ReCon (Bruker-Skyscan) software system was used for reconstruction of the 3D volumes, that are provided as stacks of bmp images for every scan. The images were digitally truncated to limit the volume to the areas surrounding discs and saved as a separate file and all scanned volumes were similarly reoriented along the sagittal plane in a 3-plane-view mode using the DataViewer (Bruker-Skyscan) software. CTAn 3D morphometry and densitometry analysis software (version 1.13.5.1; Skyscan-Bruker) was used to calculate the total surface area and volume of each disc, after a regions of interest (ROI) was user-defined around it. The disc regions within the ROIs was segmented from the background and eroded areas using a global threshold that represented the interface between the Mg alloy and the background.

Surface profilometry analysis of the extracted Mg discs

To assess the surface corrosion of the implanted disks surface profilometry analysis was conducted. The arithmetic average surface roughness (Ra) and waviness (Wa) of CrO3 cleaned Mg discs (see "The weight loss analysis of corroded discs") were measured using the Alpha-Step IQ stylus-based surface profiler (KLA-Tencor Corporation, Milpitas, CA). The Ra is the arithmetic average of the absolute values of the profile heights over the scan length.[45] The Wa is the average of the peak heights of the surface after applying low pass and high pass filtering to the primary profile.[46,47] The measurement control parameters used were as follows, a scan length of 2,500 μm with scan speed of 100 μm/s and sampling rate of 50 Hz was used. A standard 5 μm radius stylus tip was used with a 60° cone angle at contact speed of 3. The sensor range was chosen at 400 μm/23.8 pm with required stylus force of 34.4 mg and selected adjustment as center bias (optimized to measure a randomly distributed surface (for example, roughness measurement)). The data
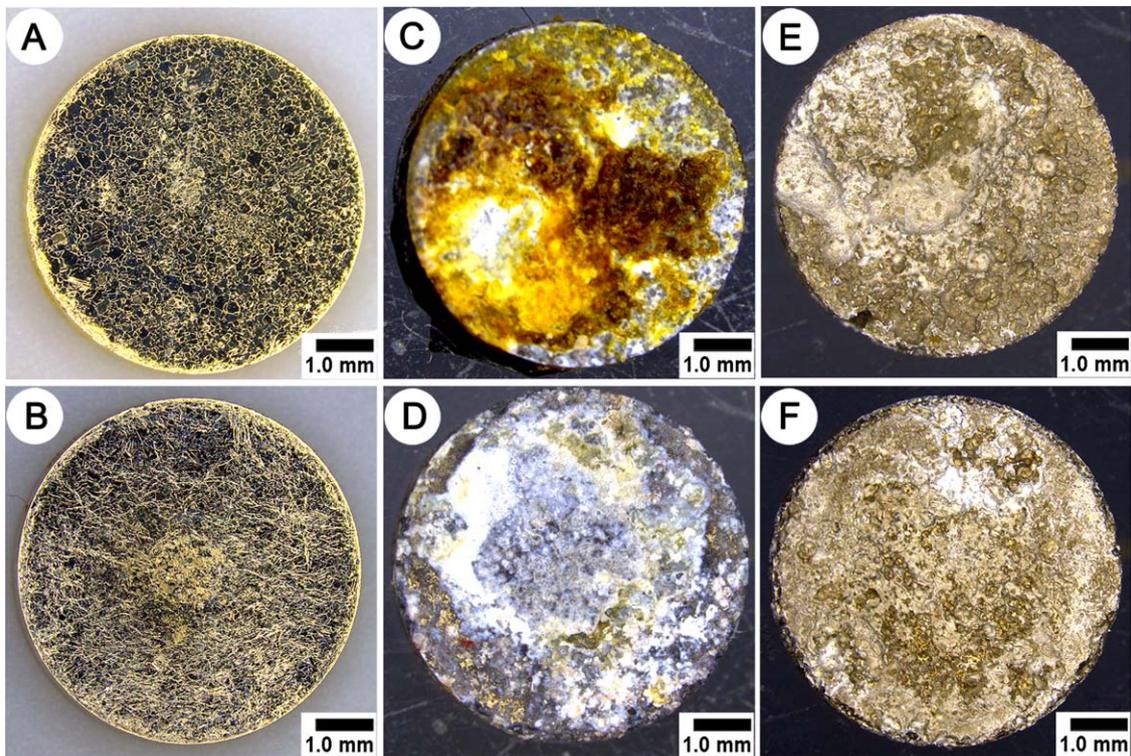
FIGURE 1. Optical images of Mg-OH and Mg-OH-AS discs as prepared (**A** and **B**, respectively), immediately after retrieval at 6 weeks *in vivo* (**C** and **D**) and after cleaning with a CrO$_3$ solution (**E** and **F**). All discs shows muscle side surface topography.

acquisition and processing was done by Alpha-Step IQ software. The collected profile was leveled using two zones method. The roughness/waviness filter cutoff (λ_c) was set at value of 25 μm and microroughness (noise) filter was turned off.

Statistical analysis
The data were compared between groups using paired *t* tests, paired *F* test of variance and the analysis of variance (ANOVA) followed by Tukey's multiple comparison test with 95% confidence level based on the assumption of normal distribution and unequal variance. All statistical analysis was performed using Origin Pro 2015 (OriginLabs, Northhampton, MA) software package. The data were presented as mean ± standard deviation (SD).

RESULTS
Light microscopy characterization of Mg discs pre- and postimplantation
The light microscope inspection of bare and AS coated Mg discs prior to implantation demonstrated that the discs did not have major defects and were free of debris [Figure 1(A,B)]. The inspection of the discs immediately after their retrieval 6 weeks postimplantation revealed that the discs were covered with organic debris and corrosion products [Figure 1(C,D)]. The inspection of the samples after CrO$_3$ treatment confirmed the complete removal of the corrosion products and organic debris from the corroded discs' surfaces [Figure 1(E,F)].

Gas pocket formation dynamics
The gas pocket analysis suggests that the AS coating effectively inhibited the gas pocket growth for the first 3 weeks, while gas pockets formed around the bare discs in the first week postoperation and their diameters increased linearly over the course of the experiment [Figure 2(A)]. At the third week postsurgery the diameters of gas pockets around the AS coated discs started to increase [Figure 2(B)]. A two-way ANOVA analysis of the data revealed that the differences between the experimental groups over 6 weeks were highly significant ($p = 0.013$). These results indicate that the AS coating effectively prevented the gas pocket formation around the Mg implant, especially in the initial postimplantation period in a subcutaneous model.

Corrosion analysis by the weight loss method
The mean percent weight loss for uncoated samples was 14.77 ± 4.60 versus 10.27 ± 1.43 (mean ± SD) for the AS coated samples [Figure 2(C)]. The paired *t* test showed that these differences approached statistical significance ($p = 0.07$), which is attributed to the large standard deviation in the percent weight loss of the uncoated samples [Figure 2(C)]. At the same time, the threefold smaller SD in the AS coated versus uncoated group suggests that the coating dramatically improves the corrosion rate reproducibility. *F* test showed significant differences in variances between the two groups ($p = 0.045$).
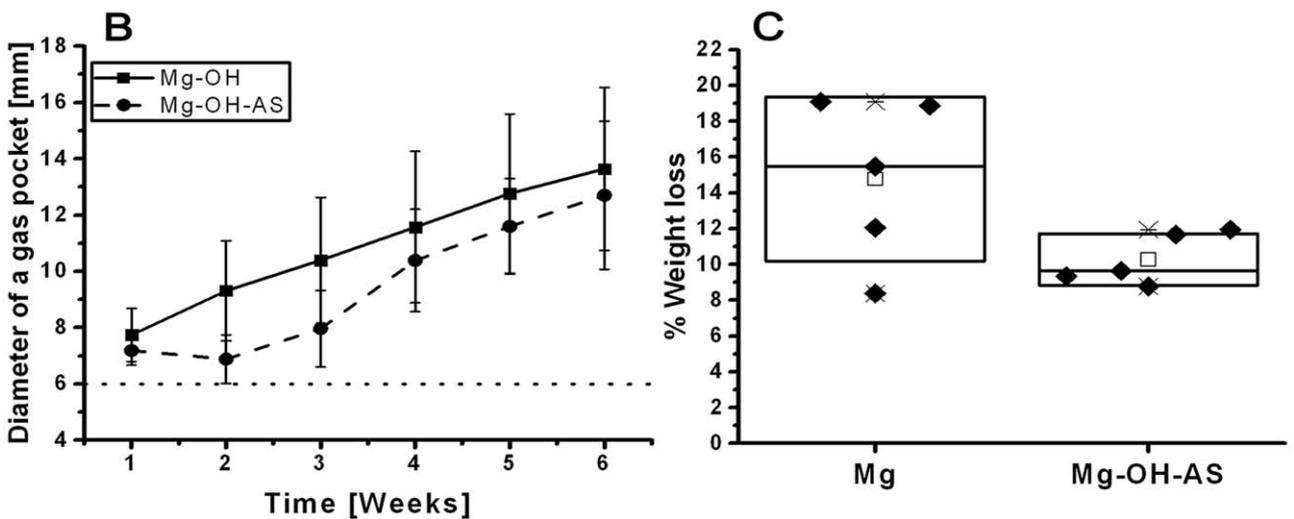
FIGURE 2. (A) Photographs of a mouse at different time points after implantation of noncoated (left side) and AS coated (right side) Mg discs. Dotted line indicates the diameter of the implanted Mg disc. (B) Changes in the diameter of the gas pockets around the AS coated (circle) and noncoated (square) Mg discs and (C) % weight loss of Mg discs implanted *in vivo* for 6 weeks. For Box plot C, the diamonds (♦) represent individual values. The median values of are represented by horizontal lines inside the box; the mean values are represented by the empty rectangle (□); the upper and lower box ranges represent standard deviation (SD).

The μCT and profilometry analysis of the corroded surfaces

The analysis of the μCT surface renderings of the corroded discs prior to the implantation revealed smooth and homogeneous surfaces for both coated and uncoated samples [Figure 3(A–D)]. The discs retrieved from the implantation sites after 6 weeks revealed significant degree of corrosion for both experimental groups [Figure 3(A′–D′)]. The degree of corrosion on the surfaces facing muscles was greater [Figure 3(A′,C′)] than on the opposite surfaces in both experimental groups [Figure 3(B′,D′)]. The corrosion patterns on the AS coated versus noncoated samples demonstrated noticeable differences. The topography of the noncoated discs was very uneven with a several deep pits, indicating the presence of pitting corrosion, while the corrosion profile of the AS coated samples was much more homogeneous, with multiple small and shallow pits evenly distributed throughout the surface.

To assess the differences in surface corrosion observed by μCT in a quantitative manner we conducted profilometry studies. Two parameters were used in the surface topography analysis of the samples. The Ra is a parameter describing surface texture at the submicron scale, while waviness Wa describes the texture at the microscopic scale. The intergroup comparison showed that Ra values were significantly higher for both surfaces in Mg-OH versus Mg-OH-AS samples ($p = 0.007$ for the surface facing the muscle side and $p = 0.042$ for the surface facing the skin side) [Table I; Figure 4(A)]. Importantly, the Ra parameters in both groups were not significantly different between the two disc surfaces, suggesting that Ra is determined by the treatment type rather than the environment. Wa mean values were close two times lower in the coated samples, although these differences were not statistically significant due to the very large variance of the noncoated samples [Table I; Figure 4(B)]. For roughness values *F* test revealed that variances in
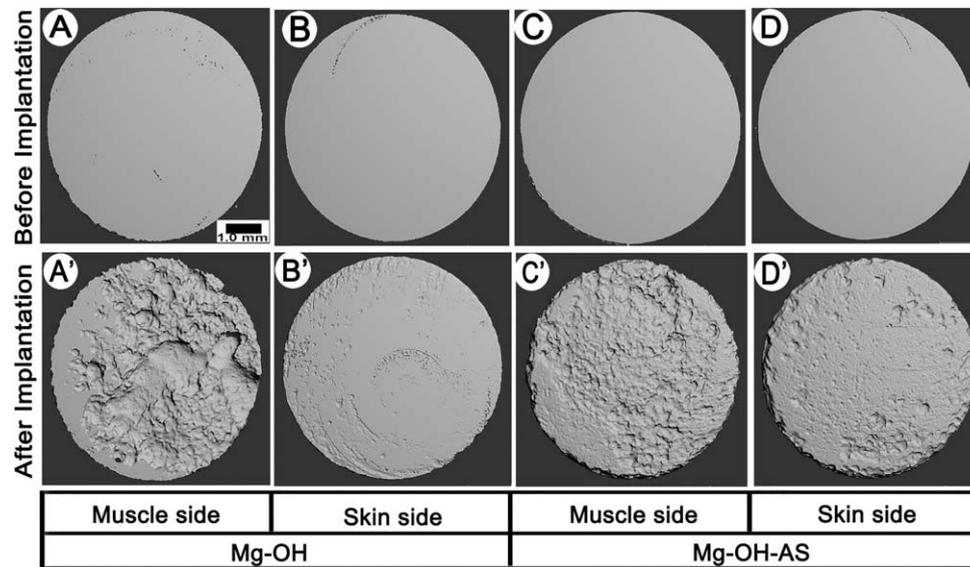
FIGURE 3. 3D μCT images of representative samples before (**A–D**) and 6 weeks after (**A′–D′**) the implantation; (**A, A′**)—muscle side and (**B, B′**)—skin side of an uncoated sample. (**C, C′**) muscle side and (**D, D′**)—skin side of a coated sample.

the coated group were significantly smaller for the coated group for skin ($p = 0.038$) but not for the muscle side ($p = 0.783$). For waviness F-test showed that variances were significantly lover in the coated group for both skin ($p = 0.004$) and muscle ($p = 0.001$) sides.

Postmortem examination and histological analysis of the sites of implantation

After euthanasia the cadavers were scanned in μCT and the sites of implantation were visually examined [Figure 5(A–C)]. No significant signs of inflammation were observed visually in the tissues surrounding the Mg-OH and Mg-OH-AS discs [Figure 5(A)]. The histological analysis of the tissue samples collected 6 weeks postimplantation from the area underneath the discs showed no differences in noncoated versus AS coated samples. Normal muscle and connective tissue appearance, similar to intact tissue, were observed in both samples [Figure 5(D–F)]. No foreign body response was observed in tissue sampled collected around the noncoated and AS coated Mg discs. These observations support the notion that the AS coatings are safe and do not cause adverse effects at the implantation sites.

DISCUSSION

The analysis of changes in gas pocket diameters clearly showed that the AS coating slowed down the formation of gas pockets. This effect was more prominent during initial 3 weeks postimplantation. These results demonstrate the feasibility of using the AS coatings for regulation of the gas pocket formation during the initial phases of the healing process. The gas pockets around implantable devices were observed in human patients[14] as well as animal models.[17,19,48,49] Several papers studied the effects of surface modifications on the gas pocket formation. Fischerauer et al. observed decrease in the gas pocket formation in the 1st 2

weeks postimplantation with the implants treated by micro-arc oxidation, however these differences were not significant and at weeks 3 and 4 the gas volume was higher than in the untreated group.[50] Interestingly, in this study a reduction of pocket size was observed beginning the 3th week postimplantation and by week 12 the pockets disappeared in both coated and uncoated groups. In our study, we did not observed any deflation of the pocket around both coated and uncoated implants. This difference might be related to the fact that the gas diffusion at the subcutaneous implantation site used in our study is much lower than at the highly vascularized bone site. This difference can be also attributed to the shorter length of our experiments. Schaller et al. studied plasma electrolytic coated implants in a craniofacial pig model.[51] Although they did not provide quantitative data, the coating decreased the gas pocket formation during 12 weeks after the implantation, based on the microCT and histological observations. In our experiments the AS coating reduced the gas pocket formation over the 6 weeks experiment in comparison to the uncoated samples, especially during the first 3 weeks postimplantation. This reduction in gas pocket diameter was highly significant, based on the ANOVA analysis. To the best of our

TABLE I. Surface Ra and Wa Values of the Mg Discs Before and After Implantation

| Sr no.	Sample	R_a (nm)	W_a (μm)
1.	Mg-OH before implantation	10.86 ± 1.10	0.47 ± 0.12
2.	Mg-OH-AS before implantation	13.98 ± 2.52	0.41 ± 0.09
3.	Mg-OH muscle side	273.43 ± 24.17	22.01 ± 18.27
4.	Mg-OH skin side	256.40 ± 37.76	15.24 ± 14.76
5.	Mg-OH-AS muscle side	206.27 ± 27.98	10.24 ± 3.73
6.	Mg-OH-AS skin side	202.10 ± 11.31	6.70 ± 2.41
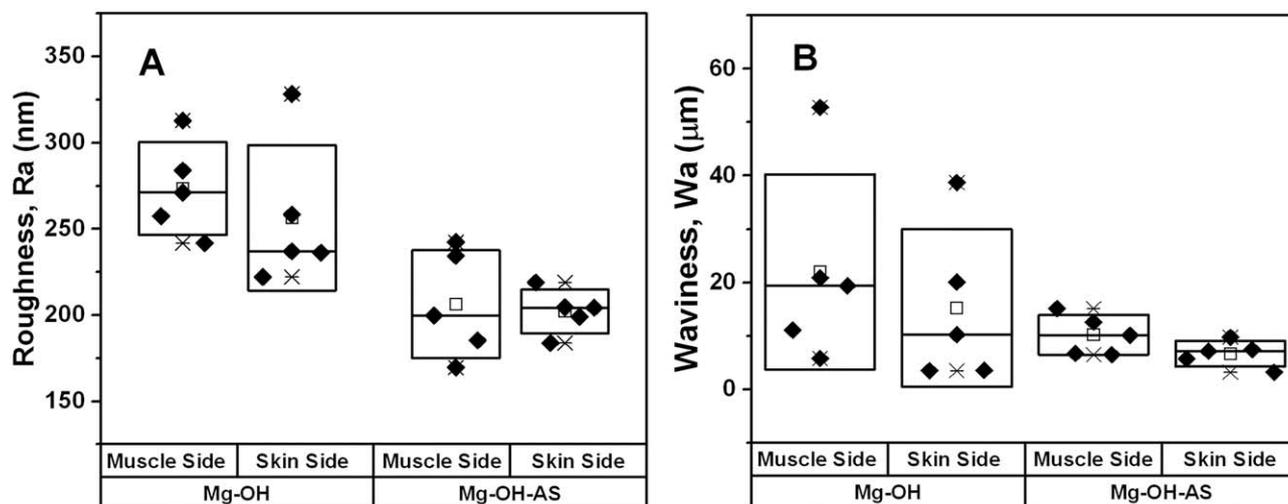
FIGURE 4. Box plots of (A) roughness (Ra) and (B) waviness (Wa) data of the samples implanted for 6 weeks after the implantation. The diamonds (◆) represent individual values from individual samples. The median values are represented by horizontal lines in the center of the box; the mean values are represented by the empty rectangle (☐) on the box plot; the upper and lower box ranges represent standard deviation (SD).

knowledge, this is a first study showing statistically significant reduction in the gas pocket size *in vivo*.

The results of our weight loss studies show $\sim$30% decrease in the mean % weight loss values in the AS coated group compared to the control. This difference however, was not statistically significant at 5% confidence level ($p = 0.07$).

FIGURE 5. Photograph of a gas pocket on back of a mouse (A), X-ray images of Mg-OH (B) and Mg-OH-AS (C) disc in mice subcutaneous region, H&E stained images of muscle tissue collected around (D) no implanted disc (control mice) (E) Mg-OH disc (noncoated), and (F) Mg-OH-AS discs (coated).

The potential reason for this might lie in the greater variation of the corrosion rates in the uncoated samples, manifested by the SD values which are three times higher in the control than that in the AS coated group. Similar trend was also observed in the Wa results showing a two times difference in the mean values between the uncoated and AS coated groups and fivefold differences in the SD values were observed in muscle side group. We hypothesize that the decrease in the SD values is due to the reduction of pitting corrosion in the coated samples. Importantly, *F* test showed that the decrease in variance of Ra and Wa values in coated samples were highly significant. The variability in the corrosion rates between Mg devices can pose significant problems for their clinical use, since this difference will affect the time these devices stay in the body. Therefore, the AS coatings can be potentially used to improve the reproducibility of the corrosion rates of the resorbable Mg devices.

The high-resolution μCT observations after the removal of the corrosion products revealed that the corroded surfaces of uncoated discs had clear signs of pitting corrosion, which is a typical mode of corrosion for Mg and its alloys.[52,53] In contrast, AS coated Mg discs corroded more homogeneously with multiple shallow dimples distributed evenly throughout the disc surface, although the corrosion was more pronounced at the edges of the discs where the coating is more susceptible to the damage. Our observations of the muscle and skin sides of the same discs in the μCT reconstructions suggested that the surfaces facing muscle side were rougher than the surfaces facing skin side in both groups, although the profilometry analysis did not show any significant differences in the Ra and Wa values between the muscle and skin (gas pocket) sides in both groups. This was unexpected, since we initially hypothesized that the mechanical forces at the interface between the discs and the muscle tissues in combination with the higher fluid access will lead to increased corrosion on the muscle side. At the same time,
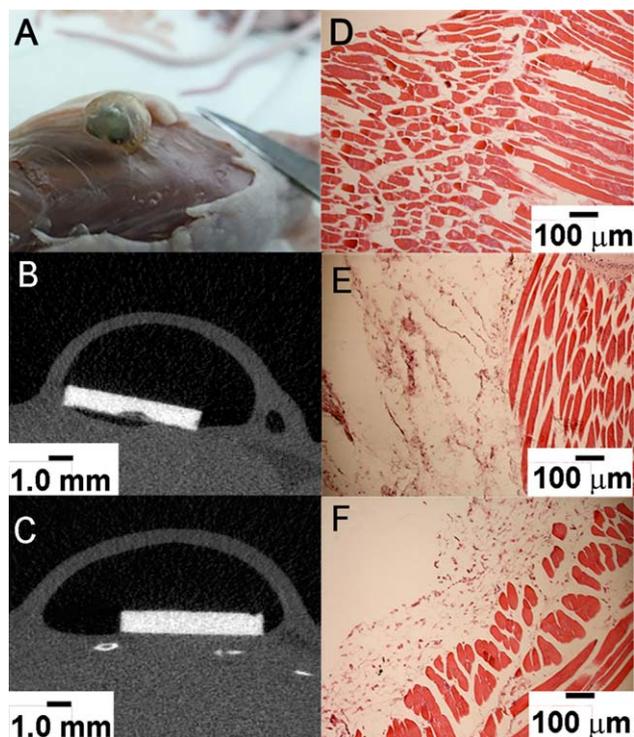
the analysis of the profilometry data revealed significant reduction in Ra values in the AS coated group. Surface roughness of implants plays important role in interaction of implants with its surrounding environment.[54,55] It has been shown that increase in surface roughness enhances the degradation rate of Mg and its alloys.[56–58] Hence, it can be of importance for clinical applications that AS coatings reduces surface roughness and the amount of pitting corrosion. We can only surmise for the mechanisms underlying this decrease in the pitting corrosion. One potential explanation will be that the coating masks the impurities and the grain boundaries which serve as nucleation sites for corrosion on the surface of the metal and therefore limiting the electrolyte access.[59]

Mg and its alloys are highly biocompatible but rapid degradation of Mg and its alloys can initiate inflammatory response in surrounding tissue at the implantation site.[48] Several *in vivo* studies reported an inflammatory tissue response to rapidly degrading implants.[60,61] Erdmann et al. noticed fibrous tissue and inflammatory cells in the surrounding tissue of MgCa0.8 alloy screws implanted in tibiae of rabbits.[60] In similar study, Abidin et al. observed foreign body reaction to products generated from degradation of pure Mg, WZ21 and AZ91 alloys when implanted in the lower back muscle of rats.[61] Reifenrath et al. noticed inflammatory tissue response when implanted ZEK100 alloy screw in lateral tibial cortices of rabbit.[48] Miura et al. also noticed little infiltration of inflammatory cells around the Mg-Al binary alloy implanted in the rat tissue.[62] Our H&E study provides an overview of the cells and tissues surrounding the implants. The degrading implants can cause myofiber degeneration that can be detected by H&E staining.[63] We did not notice any myofiber necrosis in the muscle tissue surrounding our samples, indicating that AS coating is nontoxic and does not cause a foreign body reaction. Structure of the myofibers was normal with well-defined nuclei at the implant interface as well as in the deeper layers of the muscle. In our previous *in vitro* study,[37] we have shown that, AS coating is cytocompatible[37] and our current *in vivo* data are in a good agreement with these *in vitro* experiments. It is not surprising since the degradation products of AS coating are mainly hydrocarbon (fat) and polysiloxane chains that both are biocompatible.[29] The fats can be quickly processed by the body, whereas silanes are widely used in biomedical applications and are biocompatible.[29,64]

CONCLUSIONS

In conclusion, our results demonstrate that AS coatings can effectively control *in vivo* corrosion rate of Mg discs and prevent the initial burst of H_2 gas for 3 weeks. The surface morphology study revealed that AS coated Mg discs corroded homogenously and its surface roughness was less than the noncoated Mg discs. The histology study showed no tissue damage around the AS coated Mg discs 6 weeks after implantation, which suggests that the AS coating is nontoxic and biocompatible. Overall our study demonstrates

a great potential of the AS coatings for the corrosion control of resorbable Mg implantable devices.

REFERENCES
1. Waizy H, Seitz J-M, Reifenrath J, Weizbauer A, Bach F-W, Meyer-Lindenberg A, Denkena B, Windhagen H. Biodegradable magnesium implants for orthopedic applications. J Mater Sci 2013;48(1): 39–50.
2. Reifenrath J, Bormann D, Meyer-Lindenberg A. Magnesium alloys as promising degradable implant materials in orthopaedic research. In: Czerwinski F, editor. Magnesium Alloys—Corrosion and Surface Treatments. Czerwinski F, (Ed.), InTech; 2011. DOI: 10.5772/14143. Available from: https://mts.intechopen.com/books/magnesium-alloys-corrosion-and-surface-treatments/magnesium-alloys-as-promising-degradable-implant-materials-in-orthopaedic-research
3. Staiger MP, Pietak AM, Huadmai J, Dias G. Magnesium and its alloys as orthopedic biomaterials: A review. Biomaterials 2006; 27(9):1728–1734.
4. Zhao D, Witte F, Lu F, Wang J, Li J, Qin L. Current status on clinical applications of magnesium-based orthopaedic implants: A review from clinical translational perspective. Biomaterials 2017; 112:287–302.
5. Amerstorfer F, Fischerauer SF, Fischer L, Eichler J, Draxler J, Zitek A, Meischel M, Martinelli E, Kraus T, Hann S, Stanzl-Tschegg SE, Uggowitzer PJ, Löffler JF, Weinberg AM, Prohaska T. Long-term *in vivo* degradation behavior and near-implant distribution of resorbed elements for magnesium alloys WZ21 and ZX50. Acta Biomater 2016;42:440–450.
6. Yoshizawa S, Brown A, Barchowsky A, Sfeir C. Role of magnesium ions on osteogenic response in bone marrow stromal cells. Connect Tissue Res 2014;55:155–159.
7. Yoshizawa S, Brown A, Barchowsky A, Sfeir C. Magnesium ion stimulation of bone marrow stromal cells enhances osteogenic activity, simulating the effect of magnesium alloy degradation. Acta Biomater 2014;10(6):2834–2842.

8. Rettig R, Virtanen S. Composition of corrosion layers on a magnesium rare-earth alloy in simulated body fluids. J Biomed Mater Res A 2009;88(2):359–369.

9. Witte F, Hort N, Vogt C, Cohen S, Kainer KU, Willumeit R, Feyerabend F. Degradable biomaterials based on magnesium corrosion. Curr Opin Solid State Mater Sci 2008;12(5–6):63–72.

10. Witte F, Fischer J, Nellesen J, Crostack H-A, Kaese V, Pisch A, Beckmann F, Windhagen H. In vitro and in vivo corrosion measurements of magnesium alloys. Biomaterials 2006;27(7):1013–1018.

11. Zeng RC, Cui LY, Jiang K, Liu R, Zhao BD, Zheng YF. In vitro corrosion and cytocompatibility of a microarc oxidation coating and poly(L-lactic acid) composite coating on Mg-1Li-1Ca alloy for orthopedic implants. ACS Appl Mater & Interfaces 2016;8(15):10014–10028.

12. Kuhlmann J, Bartsch I, Willbold E, Schuchardt S, Holz O, Hort N, Höche D, Heineman WR, Witte F. Fast escape of hydrogen from gas cavities around corroding magnesium implants. Acta Biomater 2013;9(10):8714–8721.

13. Witte F, Fischer J, Nellesen J, Vogt C, Vogt J, Donath T, Beckmann F. In vivo corrosion and corrosion protection of magnesium alloy LAE442. Acta Biomater 2010;6(5):1792–1799.

14. McBride E. Absorbable metal in bone surgery: A further report on the use of magnesium alloys. J Am Med Assoc 1938;111(27):2464–2467.

15. McBride ED. Magnesium screw and nail transfixion in fractures. South Med J 1938;31(5):508–515.

16. Dziuba D, Meyer-Lindenberg A, Seitz JM, Waizy H, Angrisani N, Reifenrath J. Long-term in vivo degradation behaviour and biocompatibility of the magnesium alloy ZEK100 for use as a biodegradable bone implant. Acta Biomater 2013;9(10):8548–8560.

17. Thormann U, Alt V, Heimann L, Gasquere C, Heiss C, Szalay G, Franke J, Schnettler R, Lips KS. The biocompatibility of degradable magnesium interference screws: An experimental study with sheep. Biomed Res Int 2015;2015. Article ID 943603. http://dx.doi.org/10.1155/2015/943603

18. Angrisani N, Reifenrath J, Zimmermann F, Eifler R, Meyer-Lindenberg A, Vano-Herrera K, Vogt C. Biocompatibility and degradation of LAE442-based magnesium alloys after implantation of up to 3.5 years in a rabbit model. Acta Biomater 2016;44:355–365.

19. Berglund IS, Jacobs BY, Allen KD, Kim SE, Pozzi A, Allen JB, Manuel MV. Peri-implant tissue response and biodegradation performance of a Mg-1.0Ca-0.5Sr alloy in rat tibia. Mater Sci Eng C 2016;62:79–85.

20. Gray JE, Luan B. Protective coatings on magnesium and its alloys—A critical review. J Alloys Compd 2002;336(1–2):88–113.

21. Hornberger H, Virtanen S, Boccaccini AR. Biomedical coatings on magnesium alloys: A review. Acta Biomater 2012;8(7):2442–2455.

22. Wong HM, Yeung KWK, Lam KO, Tam V, Chu PK, Luk KDK, Cheung KMC. A biodegradable polymer-based coating to control the performance of magnesium alloy orthopaedic implants. Biomaterials 2010;31(8):2084–2096.

23. Wong HM, Zhao Y, Leung FKL, Xi T, Zhang Z, Zheng Y, Wu S, Luk KDK, Cheung KMC, Chu PK and others. Functionalized polymeric membrane with enhanced mechanical and biological properties to control the degradation of magnesium alloy. Adv Healthc Mater 2017;6(8):1601269-n/a.

24. Shadanbaz S, Dias GJ. Calcium phosphate coatings on magnesium alloys for biomedical applications: A review. Acta Biomater 2012;8(1):20–30.

25. Liu X, Yue Z, Romeo T, Weber J, Scheuermann T, Moulton S, Wallace G. Biofunctionalized anti-corrosive silane coatings for magnesium alloys. Acta Biomater 2013;9(0):8671–8677.

26. Gaur S, Raman RKS, Khanna AS. In vitro investigation of biodegradable polymeric coating for corrosion resistance of Mg-6Zn-Ca alloy in simulated body fluid. Mater Sci Eng C: Mater Biol Appl 2014;42:91–101.

27. Swati G, Khanna AS, Singh Raman RK. Development of biodegradable coating for controlled dissolution of a magnesium alloy as an implant. In: Chikosha S, Chikwanda HK, editors. 7th International Light Metals Technology Conference, LMT, Vol. 828–829. Port Elizabeth, South Africa: Trans Tech Publications Ltd; 2015. pp 321–326.

28. Plueddemann EP. Chemistry of silane soupling agents. In: Plueddemann EP, editor. Silane Coupling Agents. Berlin: Springer; p 235.

29. Mojsiewicz-Pienkowska K, Jamrógiewicz M, Szymkowska K, Krenczkowska D. Direct human contact with siloxanes (silicones)—Safety or risk part 1. Characteristics of siloxanes (silicones). Front Pharmacol 2016;7(MAY). Article ID 132.

30. Chemtob A, Ni L, Croutxé-Barghorn C, Boury B. Ordered hybrids from template-free organosilane self-assembly. Chem: Eur J 2014; 20(7):1790–1806.

31. Zucchi F, Frignani A, Grassi V, Balbo A, Trabanelli G. Organosilane coatings for AZ31 magnesium alloy corrosion protection. Mater Chem Phys 2008;110(2):263–268.

32. Wang D, Bierwagen GR. Sol–gel coatings on metals for corrosion protection. Prog Org Coat 2009;64(4):327–338.

33. Zheludkevich ML, Salvado IM, Ferreira MGS. Sol–gel coatings for corrosion protection of metals. J Mater Chem 2005;15(48):5099–5111.

34. Zheng SX, Li JH. Inorganic–organic sol gel hybrid coatings for corrosion protection of metals. J Sol-Gel Sci Technol 2010;54(2):174–187.

35. Arkles B. Tailoring surfaces with silanes. Chem Tech 1977;7(12):766–778.

36. Shimojima A, Kuroda K. Structural control of multilayered inorganic-organic hybrids derived from mixtures of alkyltriethoxysilane and tetraethoxysilane. Langmuir 2002;18(4):1144–1149.

37. Patil AJ, Jackson O, Fulton LB, Hong D, Desai PA, Kelleher SA, Chou D-T, Tan S, Kumta PN, Beniash E. Anticorrosive self-assembled hybrid alkylsilane coatings for resorbable magnesium metal devices. ACS Biomater Sci Eng 2017;3(4):518–529.

38. Dorozhkin SV. Calcium orthophosphate coatings, films and layers. Prog Biomater 2012;1(1):1.

39. Park M, Lee JE, Park CG, Lee SH, Seok HK, Choy YB. Polycaprolactone coating with varying thicknesses for controlled corrosion of magnesium. J Coat Technol Res 2013;10(5):695–706.

40. Heise S, Virtanen S, Boccaccini AR. Tackling Mg alloy corrosion by natural polymer coatings—A review. J Biomed Mater Res A 2016;104(10):2628–2641.

41. Banerjee PC, Raman RKS. Electrochemical impedance spectroscopic investigation of the role of alkaline pre-treatment in corrosion resistance of a silane coating on magnesium alloy, ZE41. Electrochim Acta 2011;56(11):3790–3798.

42. Witucki GL. A silane primer—Chemistry and applications of alkoxy silanes. J Coat Technol 1993;65(822):57–60.

43. Shimojima A, Kuroda K. Designed synthesis of nanostructured siloxane–organic hybrids from amphiphilic silicon-based precursors. Chem Rec 2006;6(2):53–63.

44. Shimojima A, Sugahara Y, Kuroda K. Synthesis of oriented inorganic-organic nanocomposite films from alkyltrialkoxysilane-tetraalkoxysilane mixtures. JACS 1998;120(18):4528–4529.

45. Bhushan B. Surface roughness analysis and measurement techniques. In: Bhushan B, editor. Modern Tribology Handbook, Two Volume Set. Boca Raton, FL, 33431, USA: CRC Press LLC; 2000. p 1760.

46. Farayibi PK, Abioye TE, Murray JW, Kinnell PK, Clare AT. Surface improvement of laser clad Ti-6Al-4V using plain waterjet and pulsed electron beam irradiation. J Mater Process Technol 2015; 218:1–11.

47. Frade M, Enguita JM, Álvarez I. In situ waviness characterization of metal plates by a lateral shearing interferometric profilometer. Sensors (Basel, Switzerland) 2013;13(4):4906–4921.

48. Reifenrath J, Angrisani N, Erdmann N, Lucas A, Waizy H, Seitz JM, Bondarenko A, Meyer-Lindenberg A. Degrading magnesium screws ZEK100: Biomechanical testing, degradation analysis and soft-tissue biocompatibility in a rabbit model. Biomed Mater (Bristol) 2013;8(4).

49. Rössig C, Angrisani N, Helmecke P, Besdo S, Seitz JM, Welke B, Fedchenko N, Kock H, Reifenrath J. In vivo evaluation of a magnesium-based degradable intramedullary nailing system in a sheep model. Acta Biomater. 2015;25:369–383.

50. Fischerauer SF, Kraus T, Wu X, Tangl S, Sorantin E, Hänzi AC, Löffler JF, Uggowitzer PJ, Weinberg AM. In vivo degradation performance of micro-Arc-oxidized magnesium implants: A micro-CT study in rats. Acta Biomater 2013;9(2):5411–5420.

51. Schaller B, Saulacic N, Beck S, Imwinkelried T, Goh BT, Nakahara K, Hofstetter W, Iizuka T. In vivo degradation of a new concept of magnesium-based rivet-screws in the minipig mandibular bone. Mater Sci Eng C 2016;69(Suppl C):247–254.

52. Ghali E, Dietzel W, Kainer K-U. General and localized corrosion of magnesium alloys: A critical review. J Mater Eng Perform 2004; 13(1):7–23.

53. Xin Y, Huo K, Tao H, Tang G, Chu PK. Influence of aggressive ions on the degradation behavior of biomedical magnesium alloy in physiological environment. Acta Biomater 2008;4(6):2008–2015.

54. Hacking SA, Boyraz P, Powers BM, Sen-Gupta E, Kucharski W, Brown CA, Cook EP. Surface roughness enhances the osseointegration of titanium headposts in non-human primates. J Neurosci Methods 2012;211(2):237–244.

55. Novaes AB, Souza SLSD, Barros RRMD, Pereira KKY, Iezzi G, Piattelli A. Influence of implant surfaces on osseointegration. Braz Dent J 2010;21:471–481.

56. Walter R, Kannan MB. Influence of surface roughness on the corrosion behaviour of magnesium alloy. Mater Des 2011;32(4):2350–2354.

57. Alvarez RB, Martin HJ, Horstemeyer MF, Chandler MQ, Williams N, Wang PT, Ruiz A. Corrosion relationships as a function of time and surface roughness on a structural AE44 magnesium alloy. Corros Sci 2010;52(5):1635–1648.

58. Nguyen TL, Blanquet A, Staiger MP, Dias GJ, Woodfield TBF. On the role of surface roughness in the corrosion of pure magnesium *in vitro*. J Biomed Mater Res B Appl Biomater 2012;100B(5):1310–1318.

59. Tian P, Liu X. Surface modification of biodegradable magnesium and its alloys for biomedical applications. Regen Biomater 2015; 2(2):135–151.

60. Erdmann N, Angrisani N, Reifenrath J, Lucas A, Thorey F, Bormann D, Meyer-Lindenberg A. Biomechanical testing and degradation analysis of MgCa0.8 alloy screws: A comparative *in vivo* study in rabbits. Acta Biomater 2011;7(3):1421–1428.

61. Zainal Abidin NI, Rolfe B, Owen H, Malisano J, Martin D, Hofstetter J, Uggowitzer PJ, Atrens A. The *in vivo* and *in vitro* corrosion of high-purity magnesium and magnesium alloys WZ21 and AZ91. Corros Sci 2013;75:354–366.

62. Miura C, Shimizu Y, Imai Y, Mukai T, Yamamoto A, Sano Y, Ikeo N, Isozaki S, Takahashi T, Oikawa M, Kumamoto H, Tachi M, et al. *In vivo* corrosion behaviour of magnesium alloy in association with surrounding tissue response in rats. Biomed Mater (Bristol) 2016;11(2). Article ID 025001.

63. Xiao J, Huang C, Shi D, Zhu R, Gu R, Wang H, Wu G, Liao H. Inflammatory and immuno-reactivity in mice induced by intramuscular implants of HSNGLPL peptide grafted-polyurethane. J Mater Chem B 2016;4(10):1898–1907.

64. Kros A, Jansen JA, Holder SJ, Nolte RJM, Sommerdijk NAJM. Silane-based hybrids for biomedical applications. J Adhes Sci Technol 2002;16(2):143–155.